applied sciences

MDPI

Article

Evaluation of Influence of the Integrated Welded Handrail System in the Bus Body Frame on Strength and Passive Safety

Kostyantyn Holenko [1], Eugeniusz Koda [2], Oleksandr Dykha [1], Ivan Kernytskyy [2,3], Orest Horbay [3], Marek Chalecki [2,*], Yuriy Royko [3], Ruslan Humeniuk [4], Andrii Sharybura [5], Yaroslav Sholudko [4], Serhii Berezovetskyi [4] and Vasyl Rys [5]

1 Department of Tribology, Automobiles and Materials Science, Khmelnytskyi National University, 29016 Khmelnytskyi, Ukraine; holenkoke@khmnu.edu.ua (K.H.); duhaov@khmnu.edu.ua (O.D.)
2 Institute of Civil Engineering, Warsaw University of Life Sciences (SGGW), 02-787 Warsaw, Poland; eugeniusz_koda@sggw.edu.pl (E.K.); ivan_kernytskyy@sggw.edu.pl (I.K.)
3 Department of Equipment Design and Operation, Institute of Mechanical Engineering and Transport, Lviv Polytechnic National University, 79000 Lviv, Ukraine; orest_60@yahoo.ca (O.H.); yurii.y.roiko@lpnu.ua (Y.R.)
4 Department of Mechanical Engineering, Stepan Gzhytskyi National University of Veterinary Medicine and Biotechnologies of Lviv, 79000 Lviv, Ukraine; gumenyukrv@lnup.edu.ua (R.H.); shyv.lnau@ukr.net (Y.S.); qsikoq@gmail.com (S.B.)
5 Department of Agroengineering, Stepan Gzhytskyi National University of Veterinary Medicine and Biotechnologies of Lviv, 79000 Lviv, Ukraine; sharyburaao@lnup.edu.ua (A.S.); rysvasyl@gmail.com (V.R.)
* Correspondence: marek_chalecki@sggw.edu.pl

Abstract

Achieving the EU 2030 target of a 30% CO_2 reduction requires transitioning intercity buses to CNG- or fuel-cell-driven vehicles, and urban buses to electric vehicles. The increasing mass of roof-mounted energy systems, such as battery packs, creates additional loads on the body frame. This study investigates the integration of a welded handrail system into the bus body frame as an additional load-bearing element. A combined approach based on dynamic modeling and finite element analysis was applied to evaluate the structural body response under the UNECE R100 and R110 regulations. The results demonstrate that the structural concept significantly improves the stress–strain state of the body frame. Maximum roof displacements under $5g$ loading decreased by 34% for the gas-powered model and by 50% for the electric model, enhancing passive safety by reducing window-rack intrusion. Maximum stress decreased by 20%, shifting the stress state below the ultimate strength of S235 steel and preventing rupture. Uniform strength under vertical loading increased significantly (by 58%) due to a more favorable stress distribution within the structure. Overall, the results indicate that integrating a welded handrail truss into the bus body frame can effectively improve structural stiffness and redistribute loads within the frame.

Keywords: plastic deformations; stress–strain state; uniform strength; handrail system; roof load; passive safety; directional stability

Check for updates

Received: 2 March 2026
Revised: 17 March 2026
Accepted: 19 March 2026
Published: 21 March 2026

Copyright: © 2026 by the authors. Licensee MDPI, Basel, Switzerland. This article is an open access article distributed under the terms and conditions of the Creative Commons Attribution (CC BY) license.

1. Introduction

The planned EU targets are to reduce CO_2 by 15% by 2025 and by 30% by 2030 among trucks and buses [1], including city and intercity models with a curb weight of more than 3.5 t. To achieve climate neutrality by 2050, trucks and buses must be fully decarbonized. Zero Emission Vehicles (ZEVs), which include Battery Electric Buses (BEBs) or Fuel Cell

Electric Buses (FCEBs), are the only available technical solution enabling a rapid achievement of this requirement. Accounting for approximately 40% of the bus cost, the body requires maximum unification—the possibility of installing internal combustion engines or electric motors depends on its modification. Due to the low-floor body architecture, the optimal area for installing gas cylinders, fuel cells or battery units is the roof. Placing energy storage systems inside the passenger compartment (e.g., under the seats) is generally limited by safety and accessibility requirements defined in UNECE Regulation No. 107 as well as by passenger space constraints. In addition, seats in low-floor buses are typically suspended to facilitate cleaning and maintenance of the floor area. Locating such systems in the rear part of the vehicle is also problematic, since the engine compartment and rear overhang already accommodate propulsion and auxiliary equipment, and additional mass in this area leads to unfavorable axle load distribution. A significant increase in the load on the roof frame (more than an additional 1500–1700 kg) leads to the search for structural measures to optimize the layout strength because the window racks are not able to safely absorb the resulting loads, especially considering the dynamic coefficient k_d = 2.5. To solve this problem, it has been proposed to integrate the original welded handrail truss into the body as part of its load-bearing system. Thus, in addition to its exclusively ergonomic and supporting function for passengers, which is typical for ordinary bus handrails, the proposed system significantly increases the number of links connecting the roof with the floor part of the body and improves its overall uniform strength.

The purpose of this study is to evaluate the possibility of a structural integration of a welded handrail system into the bus body frame as an additional load-bearing element in order to increase the overall rigidity and structural safety of the vehicle. Handrails are already mandatory interior elements required by UNECE regulations to ensure passenger safety; therefore, their integration into a welded spatial truss connected to the body frame can provide additional structural capacity without increasing material costs. This approach redistributes part of the roof loads to the handrail truss, improving the uniformity of strength and structural efficiency of the bus body. An additional objective of the study is to assess whether this structural concept can facilitate the integration of roof-mounted alternative energy systems regulated by UNECE Regulations R110 and R100, with potential extension to other regulatory scenarios in future studies. In this context, the proposed approach is evaluated as a potential solution for the electrification or retrofitting of existing buses, as well as a structural concept that can be considered in the early stages of developing new bus body prototypes.

The criteria for evaluating the active safety of city buses can be completely different: starting from the visibility from the driver's workplace [2], the response of the accelerator pedal to pressure [3] or even its mechanical strength [4], and ending with several UNECE Regulations (United Nations Economic Commission for Europe). By definition, the unified provisions of UNECE R110 concern the certification of vehicles for an installation of the components of an approved type of CNG (compressed natural gas) cylinders. Therefore, before discussing the literature on bus body frame analysis, it is appropriate to outline research relevant to UNECE R110 requirements, as they govern the inertial load cases and attachment conditions for roof-mounted equipment considered in this study. Wang et al. [5] analyzed the stress–strain distribution in seamless gas cylinders through finite element modeling and experimental verification, establishing mechanical characteristics that are essential for defining UNECE R110-compliant loading and attachment boundary conditions in bus body structures. Li et al. [6] analyzed the effects of manufacturing on the mechanical properties of 34CrMo4 steel gas cylinders, yielding experimentally based material characteristics that are useful for defining strength and boundary conditions in R110-related structural analyses. Fang et al. [7] numerically analyzed the dynamic impact

response of steel gas cylinders and showed that stress concentrations predominantly arise at the cylinder-support connections, highlighting the importance of attachment design and load transfer paths in safety assessments of body structures. Wu et al. [8] developed a finite element model of a fiber-wound composite gas cylinder with an aluminum liner and demonstrated that the highest stresses and initial damage are concentrated in the transition region between the cylinder head and the barrel, identifying critical locations relevant for strength assessment and load transfer in roof-mounted systems. Park et al. [9] investigated the failure of a CNG fuel vessel in an urban bus and demonstrated that insufficient material properties can lead to catastrophic failure even in the absence of overload. These findings emphasize the importance of reliable structural integration, material quality control, and adequate safety margins for roof-mounted components governed by UNECE R110 requirements.

The purpose of this study is to evaluate the strength of the low-entry bus body frame not only under the influence of gas cylinders but also batteries (for the electric motor version), A review on the electrification of bus fleets [10] concludes that in 2020 only 0.9% of EU buses were powered electrically and 93.5% by diesel engines, which emphasizes the relevance of the EU's climate goals to reduce greenhouse gas emissions and achieve climate neutrality by 2050. Jie et al. [11] analyzed the influence of vibration and shock loads on lithium-ion batteries, providing a foundation for defining dynamic load cases and structural requirements for battery integration in electric vehicle (EV) body structures. Tran et al. [12] analyzed the vertical dynamic response of a bus subjected to harmonic road excitation and showed that suspension characteristics strongly affect body accelerations, providing justification for considering amplified vertical loads in structural analyses of bus bodies. Han et al. [13] studied the mechanical response and damage mechanisms of lithium-ion battery components under vibration and shock loading based on UN 38.3 tests and numerical models, providing insight into the structural vulnerability of battery systems integrated into vehicle bodies. Haris and Lee [14] analyzed the vibration, shock and impact behavior of a load-bearing honeycomb battery pack using finite element methods, highlighting the potential of structurally integrated battery systems to withstand dynamic loads in vehicle body applications. Bharodiya et al. [15] used finite element analysis to evaluate the structural integrity of a battery pack under impact- and shock-related load cases, showing that weight optimization can be achieved without compromising safety under mechanical abuse conditions. Chacko et al. [16] analyzed the influence of vibrations and impact-induced resonance on traction battery packs, showing that dynamic excitation affects battery behavior and highlighting the importance of accounting for vibration-related effects in the structural integration of batteries within vehicle bodies. Li et al. [17] used finite element analysis to study battery pack protection during side impact and showed that threshold beam structures play a critical role in energy absorption and intrusion reduction, directly influencing the passive safety performance of battery-integrated vehicle bodies.

The influence of ambient temperature, the load from passengers and the duration of stops affect the consumption of batteries in electric buses and their weight [18,19]. The latter indicator determines the amount of load on the bus body and requires ensuring the necessary strength margin, which is one of the tasks of the research presented below. Yao and Yang [20] performed FEA of the bus body frame using Hypermesh and Nastran to determine the strength, stiffness and modal frequency of the structure. Yang et al. [21] present an evaluation of the safety performance of a hydrogen fuel cell city bus body frame using FEA under typical operating conditions. After optimization, the maximum stresses were reduced by 20.13%. Wang et al. [22] presented an approach to designing an electric bus body using analytical target cascading (ATC) to decompose the problem into system and subsystem levels. As a result, a weight reduction of 49 kg and an increase in

torsional stiffness by 17.5% were achieved, which were confirmed by both test methods (FEA and experiment).

Issues of strength, stiffness and safety of bus bodies are also the subject of many publications. Pravilonis et al. [23] analyzed the possibility of a replacing some additional frame elements by those made of fiberglass from a point of view of the dynamic characteristics of the frame; they showed that this reduces the frame mass by 11% and shifts downward the center of gravity of the bus, while not affecting the safety characteristics. Fu et al. [24] presented an aluminum–steel body structure for an electric bus. Using the sensitivity analysis, they optimized the frame by a minimization of the total mass, whereas bending, torsional stiffness, and torsional frequency stayed unaffected to the most possible extent. Wang et al. [25] established finite element models for the electric bus body frame, considering its rollover analysis, static strength and modal analysis. Zeng et al. [26] analyzed sound and vibration propagation in the drivetrain of an electric bus. Zhang et al. [27] used the Monte Carlo method for an analysis of strength reliability of bus body frames. Teng et al. [28] analyzed a bus body frame reinforced by composite material elements. They assessed the reinforcement by crash test simulations.

Passenger comfort in city buses, including thermal microclimate, air quality and vibration levels, largely depends on the structural design of the bus body and the integration of onboard systems. Barberi et al. [29] investigated the impact of the COVID-19 pandemic on public transport use and passenger mobility, highlighting new challenges for the design and operation of urban bus systems, particularly in terms of passenger capacity and interior layout, as well as health and safety issues. Voichyshyn et al. [30] discovered the thermal behavior of a city bus interior and proposed a combined heating system based on engine heat recovery and air curtains. The study showed that the thermal characteristics of the passenger compartment were closely related to the structural design of the bus body and the integration of onboard systems. Zelenko et al. [31] analyzed the formation and monitoring of noise and vibration loads in vehicles, emphasizing the importance of structural and acoustic design solutions aimed at improving passenger comfort and environmental performance.

In addition to general considerations regarding structural design, the safety and reliability of bus body structures are significantly influenced by regulatory requirements established by UNECE regulations governing the structural integrity of vehicles and passenger safety. Bondarenko et al. [32] proposed analytical approaches for assessing the deformability and functional safety of transport infrastructure elements under operational loads, which are relevant for assessing the structural behavior and reliability of transport systems throughout their life cycle. Nguyen [33] evaluated the structural strength and passive safety of a passenger bus body frame using finite element modeling for frontal impact and rollover scenarios in accordance with the requirements of the UNECE Regulations No. 33 and No. 66. Ruban et al. [34] developed approaches for monitoring the technical condition of bus body structures during operation using non-destructive methods and finite element modeling to assess corrosion, fatigue degradation and compliance with passive safety requirements throughout the service life of buses. Finally, in previous research, Holenko et al. [35] investigated the structural integrity of battery packs installed in converted electric buses in accordance with the safety requirements of UNECE Regulation R100. The study analyzed the behavior of battery frames under high inertial loads and emphasized the importance of structural solutions that ensure the safe integration of energy storage systems. This research is closely related to the present work and complements it by considering another structural aspect of R100 compliance, namely the load-bearing capacity of the bus body frame and the potential role of the welded handrail system in increasing its rigidity and safety.

Despite the large array of scientific sources on the bus body strength or their elements employing the FEA, the authors did not find any publications devoted to the idea of integrating the system of welded handrails into the body frame. Taking into account the relevance of the unification of low-floor bodies for different powertrains, which changes the total mass by ±10–15%, the proposed research can be of practical benefit. An additional argument is the almost constant material capacity, which is extremely important for bus manufacturers given their cost and market competition.

With respect to the key assumptions and limitations of the adopted numerical model, the bus body frame was represented using beam-type finite elements with assigned tubular cross-sections corresponding to the main structural members. The material of the frame (S235 steel) was modeled using a bilinear isotropic hardening stress–strain relationship. The analysis focused on the global structural response of the body frame under regulatory loading conditions, while the connections between structural members were assumed to be rigid. Such a beam-based modeling approach is computationally efficient for predicting the global structural behavior of the bus body in crash scenarios, while avoiding the high computational cost of detailed solid models that are less suitable for rapid structural optimization (e.g., variation of tube cross-sections or joint configurations). At the same time, this simplified representation does not explicitly capture local structural effects such as joint stiffness, weld behavior, or local shell deformations, and therefore the results should primarily be interpreted at the level of global structural response of the body frame.

The proposed structural concept was evaluated using the geometry of the city bus model 4289 developed by "Ukrautobusprom". The body frame material was assumed as the S235 structural steel in accordance with the technical documentation of this vehicle, ensuring the practical relevance of the obtained results. Since the handrail truss is welded to the body frame, the use of the same material is also technologically justified from a manufacturing perspective. The cross-section of the handrails was assumed to be circular, which corresponds to ergonomic requirements related to passenger grip comfort. However, the wall thickness of the tubes may vary depending on the selected tube assortment and can be optimized in future studies. The adopted beam-based modeling approach allows such parametric variations of structural members to be investigated efficiently in further design iterations. From a structural design perspective, the proposed concept is not limited to a specific bus geometry, as the key design principle is the integration of the handrail system as a structural link connecting the main load-bearing elements of the body (roof, floor, and sidewalls), enabling efficient load redistribution within the frame.

2. Materials and Methods

To assess the strength of the bus body roof under electric batteries or gas cylinders, the Economic Commission for Europe of the United Nations (UNECE) establishes a wide range of documents. Thus, R100 rules regulate the safety of EVs: the design and placement of battery units, their protection in the event of an accident, installation and fastening conditions, etc. The R110 rules are applied to buses equipped with gas cylinders for CNG and form the basis of the boundary conditions of the studies presented below together with R100. Other regulations, such as R66, specify passenger protection during a side rollover of the bus. Adding batteries to the roof increases the COG (center of gravity) height and the resulting deformations of the inter-window racks of the body sides, which determines the remaining space of the cabin (passenger safety). If conducting a typical frontal crash test assumes the value of $k_d = 20...30g$, then according to the R100/110 regulation for vehicles of categories N3 and M3 (more than 8 seats, except for the driver's seat, with a mass of more than 5 t), the following regulatory definitions of acceleration are applied:

- $6.6g$ horizontally in the direction of motion;

- $5g$ horizontally, perpendicular to the direction of motion.

Inertial loading conditions (e.g., $5g$ and $6.6g$ acceleration) were represented using an equivalent static approach, in which the corresponding inertial forces were applied as static loads (according to R100). This approach is appropriate because the normative acceleration scenarios represent quasi-static inertial loading, which is used to evaluate global stiffness and load redistribution in the bus body frame, whereas transient or explicit analyses are primarily needed for detailed modeling of short-term impact phenomena and local structural failure. The use of standardized UNECE regulatory loading scenarios also ensures comparability of structural performance between different bus designs, since the introduction of arbitrary operational loading conditions would prevent consistent safety evaluation and certification. In practice, various real-world loading situations are addressed through different UNECE regulations (e.g., R66 rollover protection, R95 side impact, R80 seat anchorage), each defining its own verification scenarios.

At the same time, according to the official R100 description, the purpose is to check the safety characteristics of the battery pack (REESS—Rechargeable Electrical Energy Storage System) under the influence of inertial loads that may occur during an accident. Accelerations applied to REESS according to R100 are the same as those for categories N3 and M3 of R110, i.e., $6.6g$ and $5g$, respectively. This unifies the formation of boundary conditions for the calculation of the body in the following calculation cases:

- gas cylinders with a total mass of 700 kg in the fully filled state, and an air conditioner weighing 300 kg (Figure 1);
- battery pack and the same air conditioner.

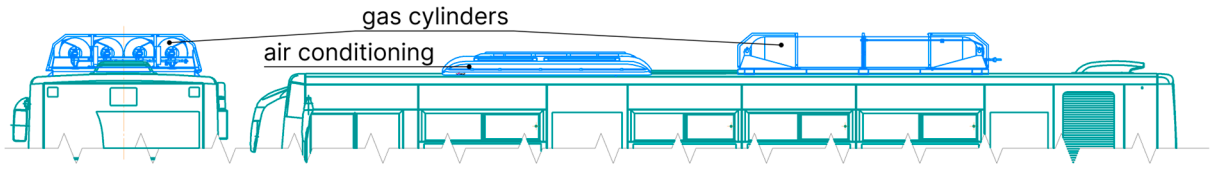

Figure 1. Diagram of location of gas cylinders and air conditioning on the roof of a low-floor bus.

For describing an electric bus, a two-mass mathematical model was suggested including: m_1 [kg]—mass of the fully equipped bus and m_2 [kg]—mass of the battery or gas cylinders (can be considered together with the air conditioner, if available). The integration of an elastic connection (damper) between m_1 and m_2 is responsible for the concept of a damped harmonic oscillator that can simulate the oscillations between these masses during an impact or heavy braking (to achieve $6.6g$ in the direction of motion). The complexity of this mathematical model is increased by the sequence of energy absorption and its transfer from m_1 to m_2: the bus body undergoes acceleration, which is transmitted from its lower part to the batteries on the roof. For simplicity, it has been considered as a one-dimensional system along the impact axis. The dynamic equations for a system subjected to an external impact force $F_{ext}(t)$ and including two masses, a spring and a damper can be expressed as a set of coupled differential equations:

- for m_1:

$$m_1\ddot{x}_1 + c\left(\dot{x}_1 - \dot{x}_2\right) + k(x_1 - x_2) = F_{ext}(t) - F_{dis}(t), \quad (1)$$

- for m_2:

$$m_2\ddot{x}_2 + c\left(\dot{x}_2 - \dot{x}_1\right) + k(x_2 - x_1) = F_{trans}(t), \quad (2)$$

where x_1, x_2 [m]—displacements of m_1 and m_2 related to their positions of equilibrium; $\dot{x}_1$, $\dot{x}_2$ [m/s]—velocity of m_1 and m_2; $\ddot{x}_1$, $\ddot{x}_2$ [m/s^2]—acceleration of m_1 and m_2; $F_{ext}(t)$ [N]—time-dependent external force applied to m_1 during impact (or braking); k [N/m]—stiffness of the connection between the body and the batteries; c [N·s/m]—damping coefficient (dissipation of energy in the system in the form of movement resistance between masses, simulating the effect of structural deformation, friction and other forces that dissipate energy); $F_{trans}(t)$ [N]—the force transferred to m_2 as a function of a time delay (τ) and efficiency factor (η) modeled to represent the energy transfer process from m_1 (gradually increasing from 0 to a maximum value, reflecting the progressive engagement of the spring-damper system); and $F_{dis}(t)$ [N]—the force contributing to the dissipation of energy during the impact.

In the simplest case, $F_{dis}(t)$ is an exponential decay function representing the decrease in energy as it is absorbed by the bus body frame or the force associated with energy dissipation (dissipation or damping):

$$F_{dis}(t) = F_0 \cdot e^{-\lambda t} \text{ or } F_{dis}(t) = c \cdot \dot{x}(t). \quad (3)$$

where F_0 [N]—initial force at the moment of impact; $e^{-\lambda t}$—represents an exponential decrease with time, where λ [s^{-1}] is a constant characterizing the rate of energy dissipation; t [s]—time; $\dot{x}(t)$ [m/s]—the object velocity at a time instant t. In fact, $F_{dis}(t)$ can be a complex multivariate function describing the specific configuration of the bus body frame (number of battery mounting points, taking into account the position of their COGs relative to the bus axes, etc.), and is the subject of future research.

The energy balance equation of the system $E_{total}(t)$ for this model contains the kinetic energy, potential energy, dissipation energy due to damping (from the beginning of the process to the time instant t), and additional energy losses $E_p(t)$ due to plastic deformations:

$$E_{total}(t) = \frac{1}{2}m_1\dot{x}_1^2 + \frac{1}{2}m_2\dot{x}_2^2 + \frac{1}{2}k(x_1 - x_2)^2 + \int_0^t c\left(\dot{x}_1 - \dot{x}_2\right)^2 dt - E_p(t). \quad (4)$$

As a result of Transformation (4), the total energy $E_{total}(t)$ in the kinetic energy of the batteries with the mass m_2, it is possible to determine the acceleration a_b:

$$a_b = \frac{dv}{dt} = \frac{d}{dt}\left(\sqrt{\frac{2E_{total}(t)}{m_2}}\right) = \frac{1}{m_2} \cdot \frac{dE_{total}(t)}{dt} \cdot \sqrt{\frac{m_2}{2E_{total}(t)}}. \quad (5)$$

The actual boundary conditions of the bus body frame according to R110 in the FE analysis require application of a force $F_{R110} = m_2\, a_b$ at the battery attachment points. Thus, in addition to determining the acceleration a_b, it is necessary to calculate the value of the mass m_2. For the M3 category electric city bus consuming 1.5 kWh of energy per 1 km on average and having the range of 250 km (daily route range), the total energy demand will be 375 kWh. Based on the fact that the batteries have the power density of 200 Wh/kg, the approximate weight of the necessary batteries is around 1875 kg. The initial parameters are listed in Table 1, where the following notation is used: m_i—the mass of aggregates; n—the number of attachment points; k_d—the dynamic coefficient (or the above-described a_b, if the customer requires specific conditions other than R100/110); ΣF—total load; F_i—distributed load. The presence of a handrail system in the calculation model for each of the modes is indicated by the letter H in its name. For example, load modes 1.1H and 1.1 (Table 1) are characterized by identical loading conditions but differ in the body frame configuration: case 1.1H includes the welded handrail truss, whereas case 1.1 represents the conventional bus body structure without handrails. The objective is to quantify the

influence of the handrail system on the stress–strain state of the bus body under equivalent loading conditions.

Table 1. Boundary load conditions of the bus body frame.

Mode	Unit	m_i [kg]	n	k_d	ΣF [N]	F_i [N]	Axis
1.1H/1.1	air conditioning	300	9	6.6	19,423.8	2158.2	y
	gas cylinders	700	9	6.6	45,322.2	5035.8	y
1.2H/1.2	air conditioning	300	9	5	14,715	1635.0	x
	gas cylinders	700	9	5	34,335	3815.0	x
2.1H/2.1	air conditioning	300	9	6.6	19,423.8	2158.2	y
	batteries	1875	9	6.6	121,398.8	13,488.8	y
2.2H/2.2	air conditioning	300	9	5	14,715	1635.0	x
	batteries	1875	9	5	91,968.75	10,218.8	x
3.1H/3.1	air conditioning	300	9	2.5	7357.5	817.5	z
	gas cylinders	700	9	2.5	17,167.5	1907.5	$-z$
3.2H/3.2	air conditioning	300	9	2.5	7357.5	817.5	$-z$
	batteries	1875	9	2.5	45,984.4	5109.4	$-z$

Modes #3.1 and #3.2 are the particular cases separate from R100/110 and consider a vertical load F_i with k_d = 2.5 in the direction of the gravity force G (along the Z axis). Such conditions simulate the motion of a bus on a low-quality road surface with a large amplitude of irregularities, the oscillations of which generate a vertical acceleration which is over twice the gravitational acceleration g in static conditions and is transferred from the suspension to the bus body. In all cases (#1.1–#3.2), the equipped mass of the bus (8030 kg) is added to the calculation model.

The mathematical model equations for modes #3.1 and #3.2 assume a vertical load from batteries or gas cylinders and air conditioners with the coefficient k_d, and considers the influence of the handrail system on the resulting body strength:

$$F_{hr} = \sum_{i=n+1}^{n+m} G_{total} \cdot k_d \cdot W_i, \quad (6)$$

where F_{hr} [N]—part of the total weight G_{total} attributed to the handrail; G_{total} [N]—total weight of air conditioner and batteries (or gas cylinders); n—number of window racks; and m—number of vertical pipes of the handrail system (supports).

Moreover

$$W_i = \frac{w_i}{\sum_{j=1}^{n+m} w_j} = \frac{1}{\sqrt{(x_i - x_{cm})^2 + (y_i - y_{cm})^2}} \frac{1}{\sum_{j=1}^{n+m} w_j} \quad (7)$$

is a normalized weight factor of the i-th rack—the ratio which considers the proximity to batteries and ensures that the total distributed load does not exceed G_{total}. In the formula for W_i, the following notation has been introduced: w_i—individual weight factor for the i-th rack (value being the inverse of the distance between COG of the battery and the rack and having to ensure load distribution considering the proximity of the rack to the battery); w_j—the weighting factor for the j-th rack (the summation for all j from 1 to n, i.e., all individual weighting factors for each rack, visible in the denominator, is used to normalize the weights); x_i and y_i [mm]—coordinates of each rack and handrail, where i varies from 1 to $n + m$; x_{cm} and y_{cm} [mm]—coordinates of COG of the batteries.

The margin of strength SF (safety factor) of the *i*-th handrail (or rack) can be determined according to the following criterion:

$$SF = \frac{\sigma_y}{\sigma_{vm}} = \frac{S_{lim} \cdot A_i}{G_{total} \cdot k_d \cdot W_i}, \quad (8)$$

where σ_y [MPa]—a certain stress limit (as a rule, the yield limit S_{lim}); σ_{vm} [MPa]—actual von Mises stress (to simplify the calculation, it can be assumed that the axial load is the main factor in the stresses); and A_i [mm^2]—an area of the *i*-th handrail (or rack).

It has been also proposed to introduce a relatively new parameter in the strength assessment practice, based on the FEA model indicators—the strength uniformity of the structure SU (strength uniformity [MPa]) based on the mean square deviation of the von Mises stresses (σ_{max}, σ_{min}, σ_{ave}—maximum, minimum and average):

$$SU = \sqrt{\frac{1}{N}\sum_{i=1}^{N}(\sigma_i - \mu)^2}, \quad (9)$$

where σ_i [MPa]—an individual value in the data set (σ_{max}, σ_{min}, σ_{ave}); N—the number of values in the data set (in this case, it can be accepted $N = 3$); and μ—arithmetic average of all values.

The proposed strength uniformity (SU) parameter characterizes the degree of uniformity of stress distribution within the bus body frame. Unlike traditional assessments based solely on maximum stress values, SU allows the evaluation of how evenly the loads are distributed throughout the structure. The parameter is intended as a simplified comparative engineering indicator for assessing load redistribution between different structural configurations rather than a full statistical description of the stress field in the FE model.

The logic of the SU indicator is as follows: the smaller the difference between the moduli of the maximum, minimum and average stresses, the more uniform their distribution on the model. SU determines the efficiency of the bus body design and allows the estimation of it section by section: roof, floor part at the chassis level, sidewalls, front and rear overhangs, etc. The development of this direction can be the topic of future research.

The bus body frame was processed using a finite element mesh generated in ANSYS (2023 R1) Mechanical with an average element size of approximately 16.8 mm. The final finite element model consisted of 68,247 nodes and 35,297 elements, ensuring adequate resolution of the stress–strain state of the beam structure (BEAM189 and BEAM188 types of the finite elements). The average element quality was approximately 0.996, with a minimum value of 0.798, indicating a high-quality mesh suitable for structural analysis. The average aspect ratio of the elements was approximately 1.03, while the maximum value did not exceed 1.39. The Jacobian ratio remained close to unity (average $\approx$ 0.994), and the average skewness of the elements was about 0.016, indicating minimal element distortion. These parameters confirm that the generated mesh satisfies the requirements for accurate finite element analysis of frame-type structures.

Experimental validation of the proposed structural concept was not performed within the scope of the present study. Regulatory verification scenarios associated with UNECE Regulations R100 and R110 involve high inertial loads that typically lead to plastic deformations of the bus body frame, which in practice results in irreversible structural damage and the necessity of subsequent disposal of the tested prototype. Considering that the body structure accounts for ~40% of the total bus cost and that prototype vehicles may cost several times more than serially produced units, full-scale experimental testing for each design iteration is economically impractical.

In addition, modern bus structures must comply with multiple safety regulations (e.g., UNECE R66 rollover protection, UNECE R95 side impact), each of which requires separate

destructive verification scenarios. Therefore, the primary objective of this study was to use finite element simulations to identify the structural tendencies associated with the integration of the welded handrail system and to compare the resulting behavior of the bus body frame under different loading regimes before costly experimental validation becomes necessary. Detailed validation using higher-fidelity solid models (instead of the beam-based modeling approach, which is computationally efficient at predictive design stages) and experimental testing may be considered at later stages of structural optimization.

3. Results

The above parametric mathematical modeling is an effective step preceding FEA to approximate the loads, accelerations, number of vertical racks of the handrail system, etc. The following FEA analysis was undertaken in ANSYS Static Structural. The rod model of the body frame of the low-entry bus (model 4289 by "Ukrautobusprom") is represented by the cross-sections (Figure 2a): 40 × 40 × 3, 60 × 40 × 3, 80 × 40 × 3, 140 × 60 × 3 mm etc. The system of handrails is welded from the pipes with a round section of 30 × 3 mm (yellow rods in Figure 2a).

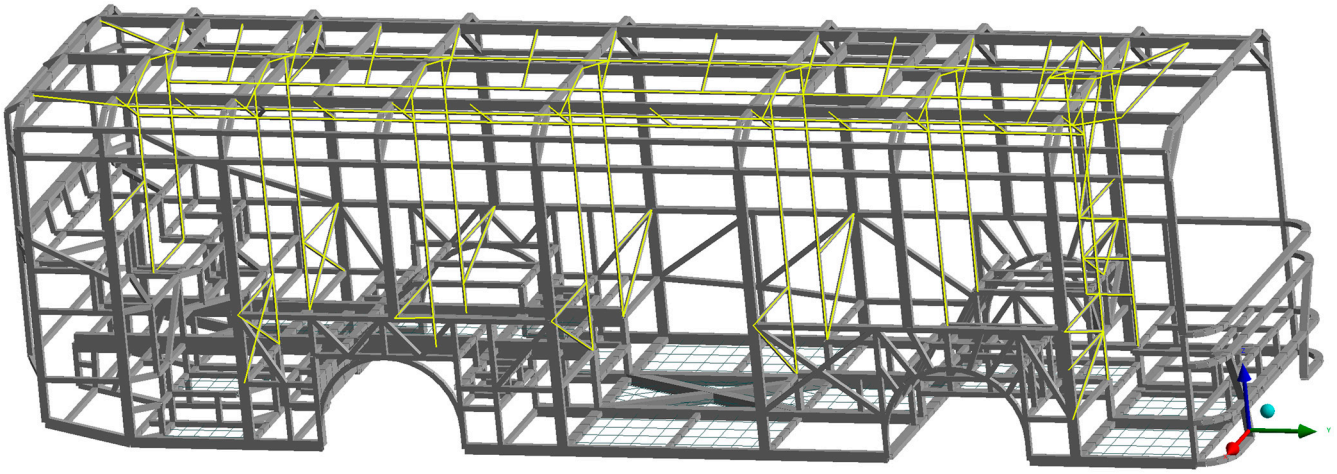

(**a**)



(**b**)

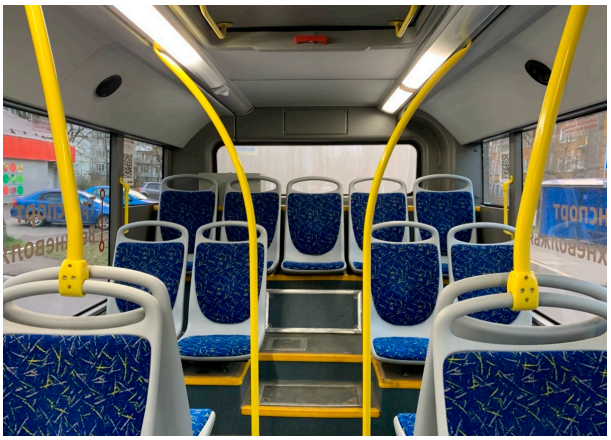

(**c**)

Figure 2. City bus body: (**a**) ANSYS rod frame of the "Ukrautobusprom" bus (model 4289) with highlighted handrail system; (**b**,**c**) examples of handrails of other existing city buses.

In both cases, the vertical pipes of the handrails rest against the frames of the seat backs (Figure 2b,c), which are made of plastic. Thus, it becomes obvious that such handrails do not perform any force connection between the floor and the roof—instead, their function is solely to support passengers. An additional confirmation of this fact is the separation of

the vertical handrails in another model (Figure 2c), where the handrails are not connected to each other by horizontal pipes; that is, the concept of a truss in this case is not considered at all. It can be assumed that if the roof is loaded with the aforementioned gas cylinders or battery blocks, vibrations and vertical accelerations will be transmitted through the handrails to the seat backs.

The boundary conditions of the FEA model have been formulated with use of the example of the calculation mode #1.1 (Table 1):

- fixed support—constraints on the mounting flanges of the air cylinders of the front suspension (tag A in Figure 3);
- displacement—restriction of movements with one degree of freedom (along the Y axis—the longitudinal axis of the bus) to enable physical deflection and stretching of the bus body under the transverse loads (tag B in Figure 3);
- standard Earth gravity—vertical acceleration g = 9.8066 m/s^2;
- air conditioning—longitudinal load ΣF (19,424 N in mode #1.1) considering k_d = 6.6, applied at six points (tag C in Figure 3);
- gas cylinders—longitudinal load from gas cylinders ΣF (45,322 N in mode #1.1) considering k_d = 6.6, applied at six points (tag D in Figure 3);
- material—S235 steel with a stress–strain curve of "Bilinear Isotropic Hardening" types with yield strength σ_y = 250 MPa and G = 1.45 GPa (tangent modulus);
- load from aggregates: 2680 kg in the rear overhang, 1235 kg in the front part and 4115 kg distributed over the body with cladding, etc. (grey spheres in Figure 3).

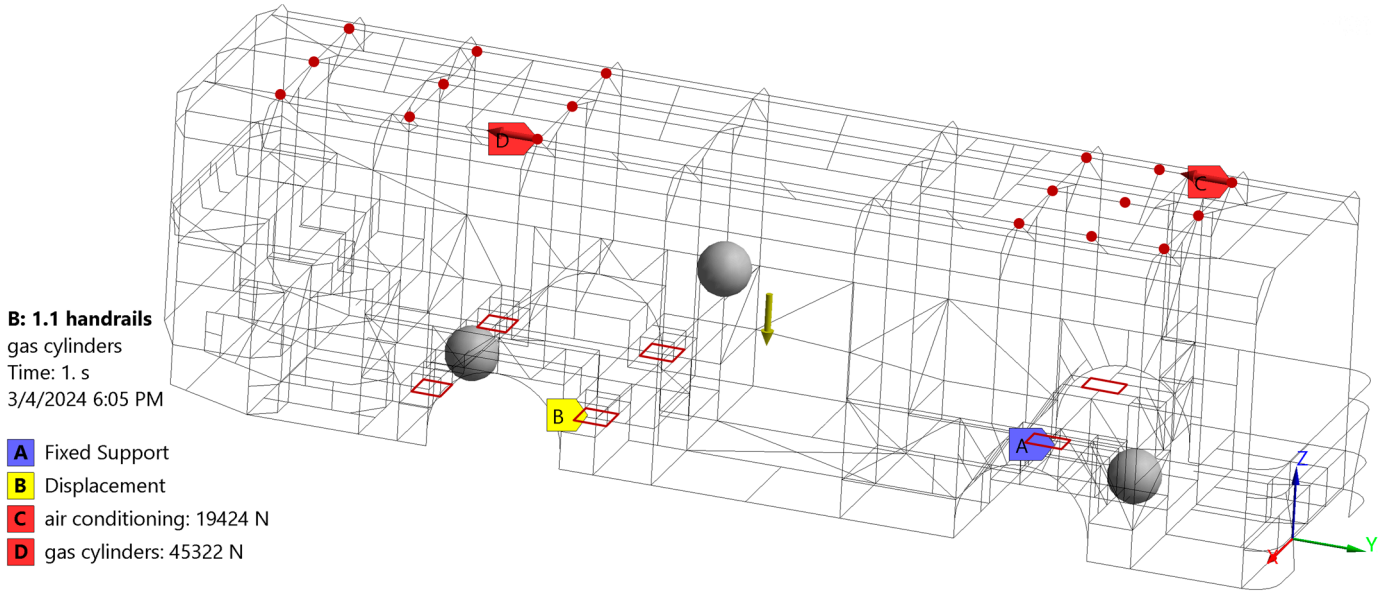

Figure 3. Boundary conditions applied to the ANSYS body frame model for the example of mode #1.1H (air conditioning and gas cylinders load with k_d = 6.6 and handrails).

Each calculation case is presented in two versions: with the handrail system (Figure 2a) and without it. The presence of a handrail system is indicated by the letter H in the name of the mode. Thus, 12 types of calculations were carried out to provide a comprehensive assessment of the body frame strength in the ANSYS Static Structural environment.

The key criteria of the evaluation of effectiveness of the handrail system integration into the body frame as a welded part of it will be the maximum and average von Mises stresses σ_{max}, σ_{ave}, the maximum and average displacements Δ_{max}, Δ_{ave}, as well as the minimum and average safety factor SF_{min}, SF_{ave} related to the yield strength σ_y = 250 MPa. Each of these three indicators has been analyzed sequentially by a comparison of the

FEA results for modes #1.1–3.2 (Figure 4) for the upper part of the body frame (above the window frame).

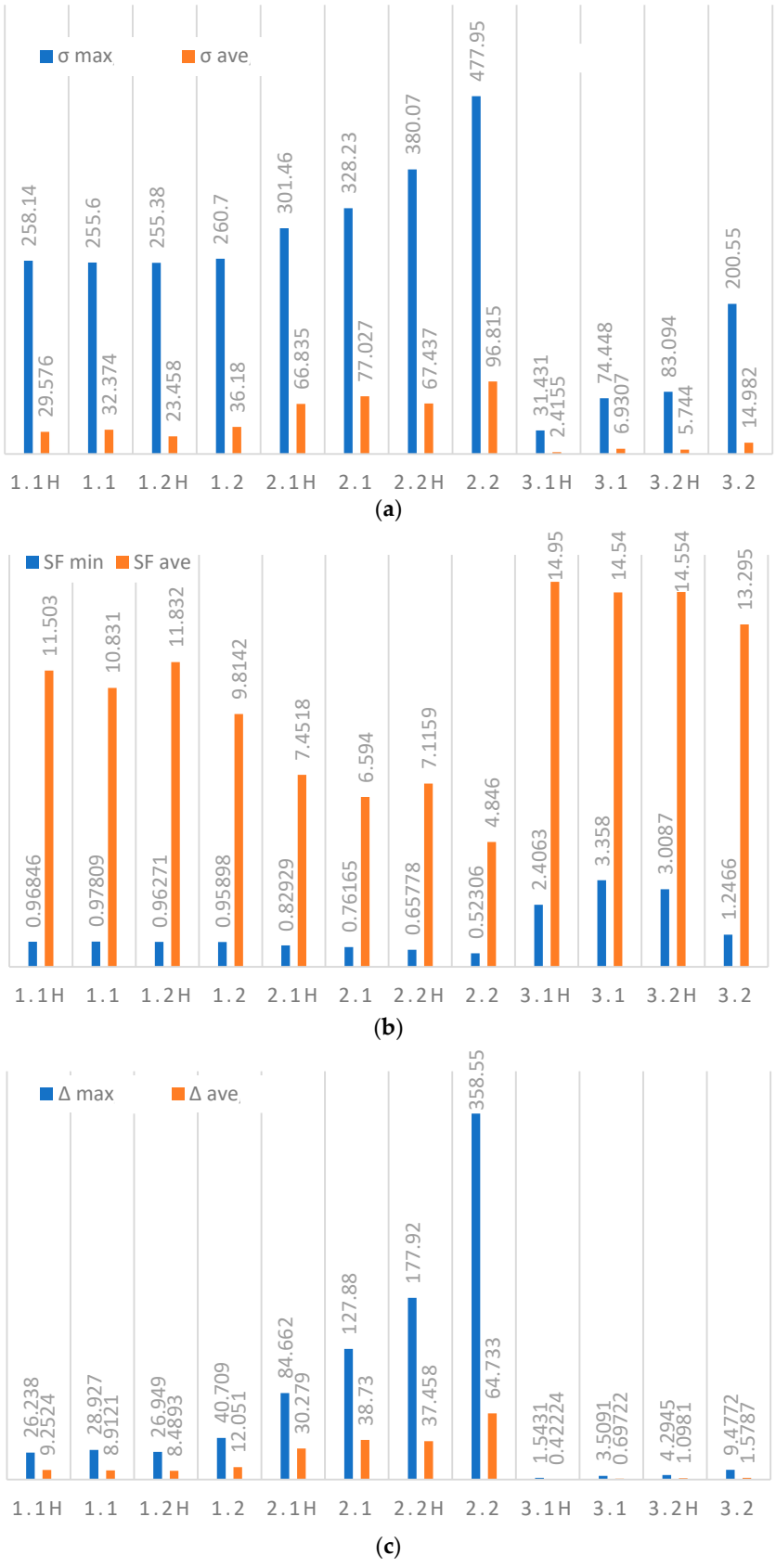

Figure 4. Parameters of the upper part of the body frame depending on the test mode: (**a**) σ_{max} and σ_{ave} [MPa] (**b**) SF_{min} and SF_{ave}; (**c**) Δ_{max} and Δ_{ave} [mm].

The situation in mode #1.1 is typical compared to other more loaded cases: the presence of handrails did not significantly improve the strength of the upper part of the body frame, moving the location of σ_{max} from the 6th window rack (tag "max" in Figure 5a) to the 3rd one (Figure 5b). The value of σ_{max} even increased by 1% to 258.14 MPa; however, the presence of handrails reduced the average stresses σ_{ave} by 8.64% (from 32.3 to 29.5 MPa), making it more uniform with respect to strength. The color scale represents the distribution of von Mises stress within the bus body frame (Figure 5).

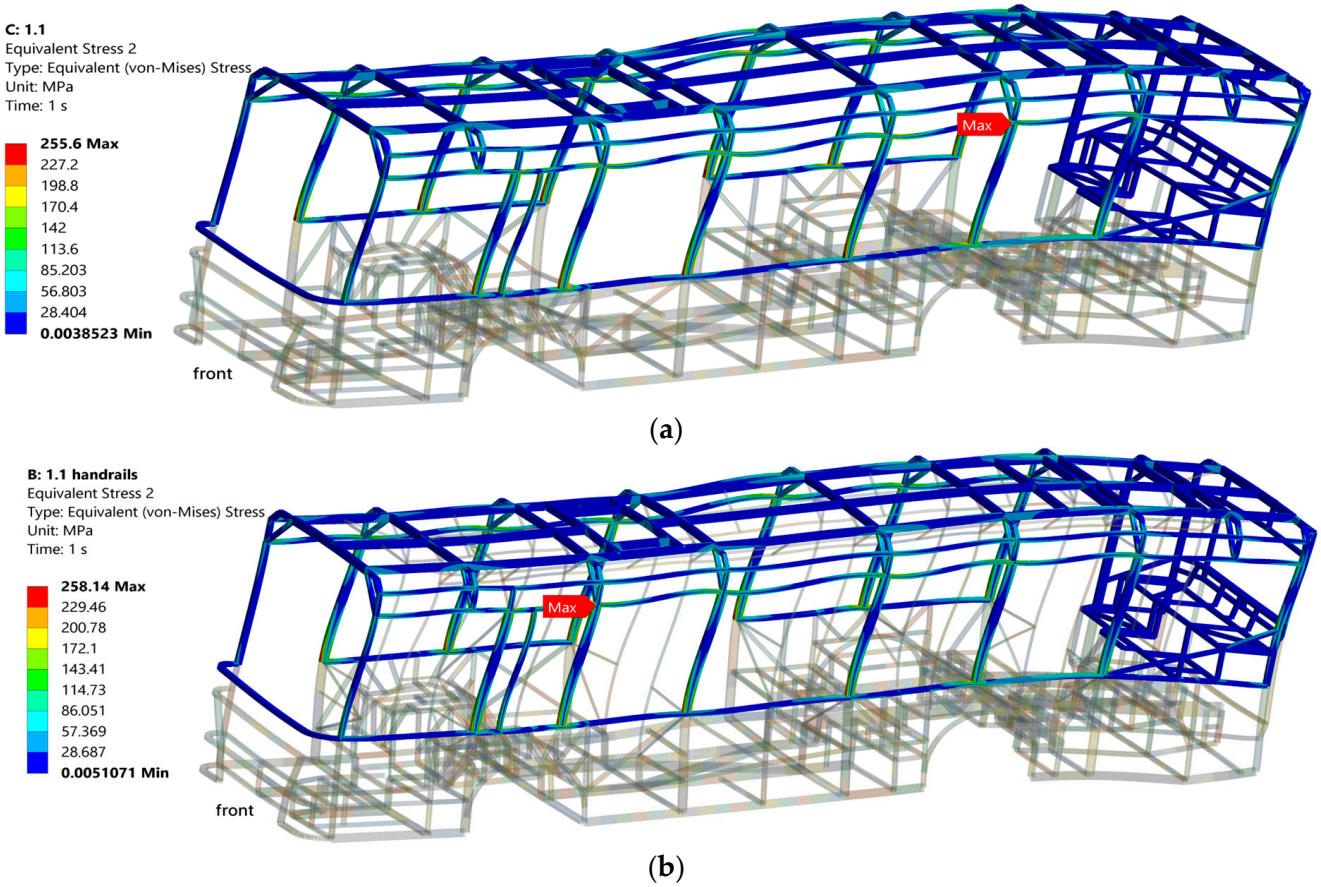

Figure 5. Von Mises stress in mode: (**a**) #1.1 (air conditioning and gas cylinders load with k_d = 6.6); (**b**) #1.1H (air conditioning and gas cylinders load with k_d = 6.6 and handrails).

The handrail system in mode #1.2 with the transverse application of the acceleration 5*g* to the model with air conditioning and gas cylinders presented a much better effectiveness: σ_{max} and σ_{ave} decreased by 2% (from 260.7 to 255.38 MPa) and 35% (from 36.18 to 23.46 MPa), respectively. The maximum deformations Δ_{max} decreased from 40.7 to 26.9 mm (Figure 6).

In the next tests, the gas cylinders have been replaced by a battery pack, increasing the mass from 700 to 1875 kg. Thus, the maximum stress σ_{max} is 301.46 MPa in mode #2.1H, which is 8.16% lower than the similar parameter in #2.1 (without the handrail system). The higher load of mode #2.1 is also evidenced by the indicator SF_{min}, which is 0.83 for the model with handrails (#2.1H) and only 0.76 without handrails (#2.1). This is significantly lower than 0.97 for #1.1H, but in both cases it means the appearance of local plastic deformations.

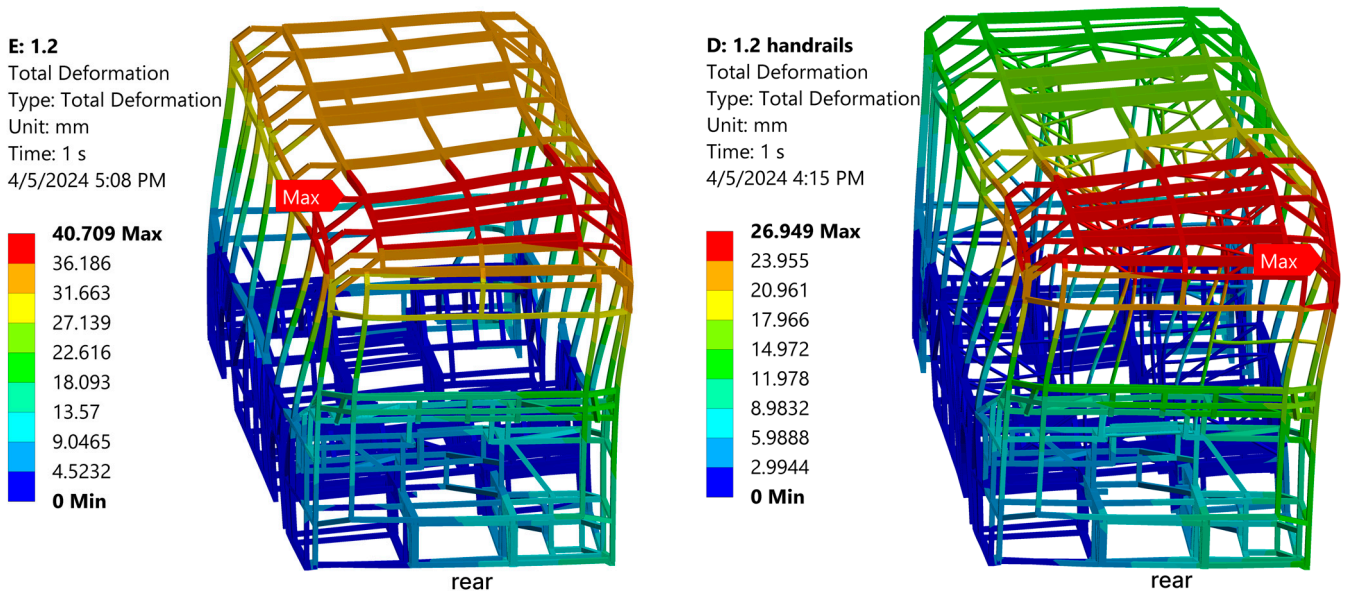

Figure 6. Body frame deformations in mode: (**a**) #1.2 (air conditioning and gas cylinders load with k_d = 5), (**b**) #1.2H (air conditioning and gas cylinders load with k_d = 5 and handrails).

Thanks to the introduction of the handrail system into the body frame structure, the deformation value Δ_{max} was reduced from 127.88 (#2.1) to 84.66 mm (#2.1H) (Figure 7; the color scale indicates the magnitude of structural displacements).

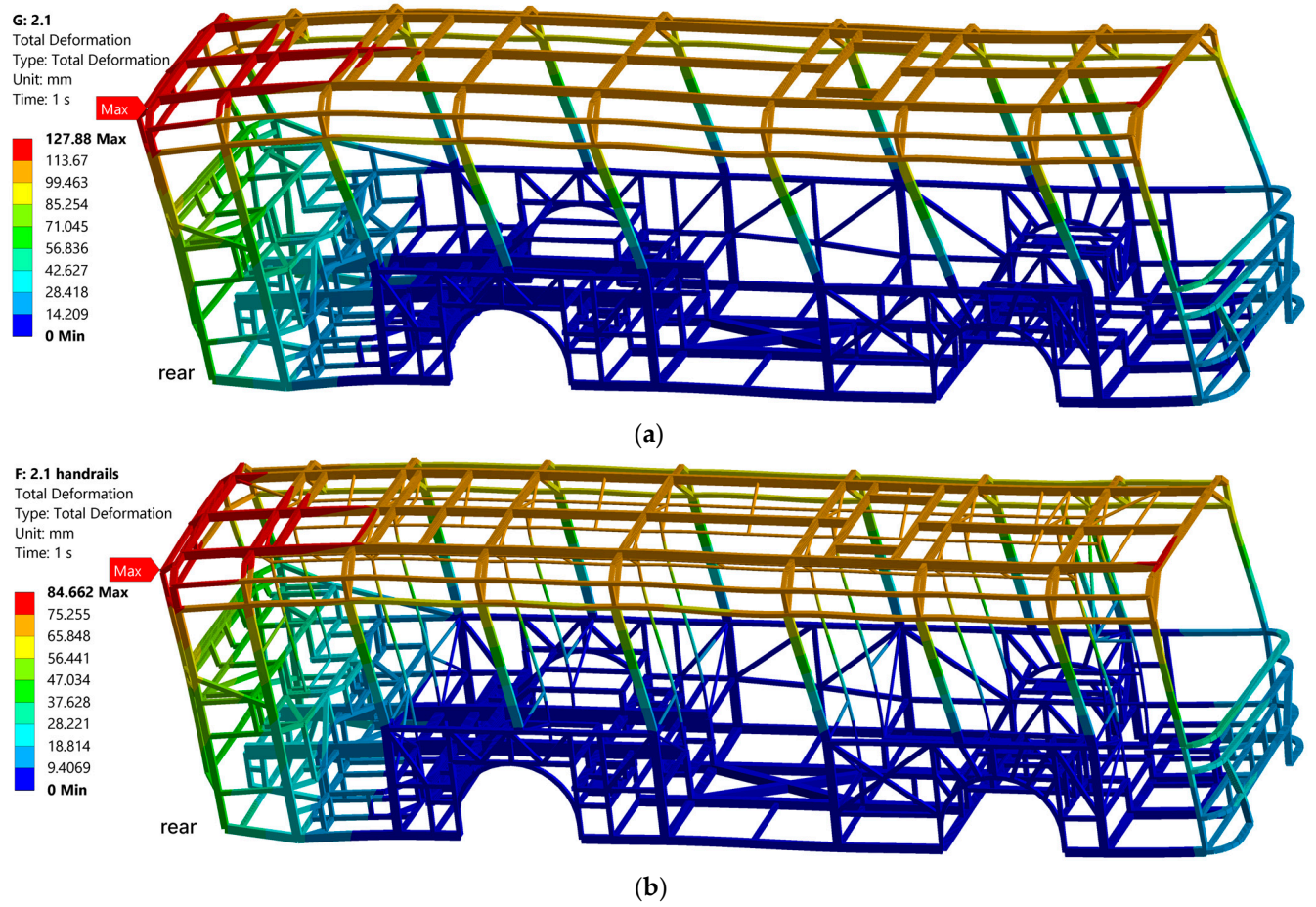

Figure 7. Comparison of deformations in modes: (**a**) #2.1 (air conditioning and batteries load with k_d = 6.6); (**b**) #2.1H (air conditioning and batteries load with k_d = 6.6 and handrails).

The last test mode #2.2 for compliance with R100/110 under the transverse acceleration of 5*g* proved to be the most difficult. To determine the impact of the weight increase from 700 to 1875 kg, both "transverse" modes (#1.2H and 2.2H) have been compared with respect to the stresses of the welded handrail system itself: 259.68 MPa vs. 337.76 MPa (Figure 8), respectively. On the one hand, this indicator is quite high, and on the other it clearly demonstrates the effectiveness of handrails and the stress transfer from the body to them.

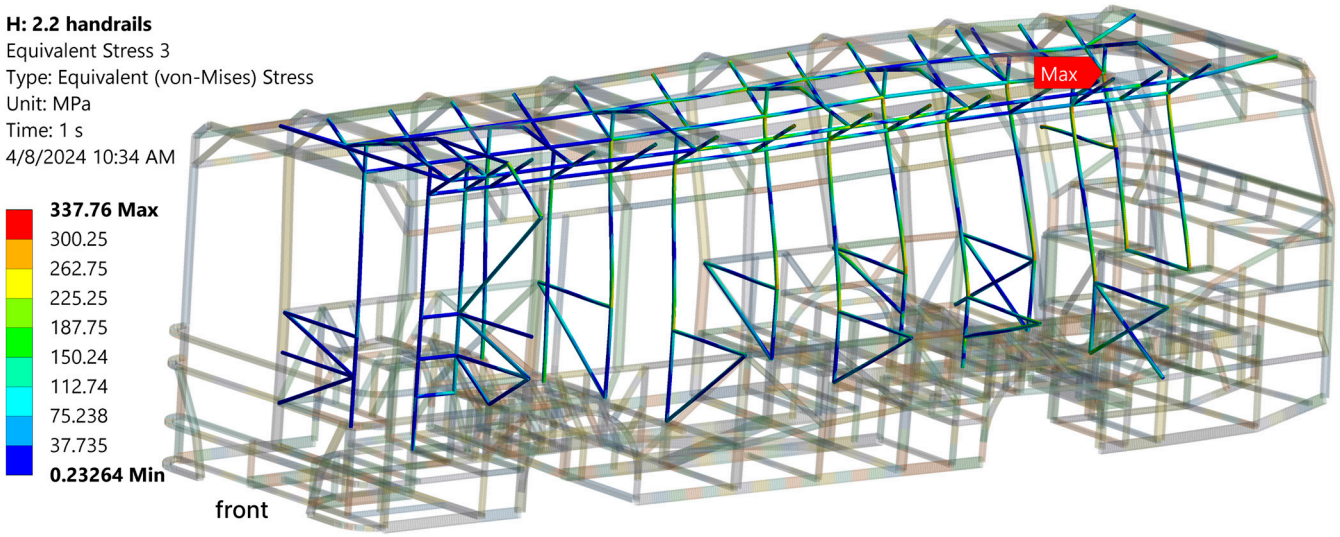

Figure 8. Von Mises stress map of the handrail system in mode #2.2H (air conditioning and batteries load with k_d = 5 and handrails).

The values of the maximum deformations of the handrail system between the modes #1.2H and 2.2H differ by more than 6 times: 26.18 vs. 176.29 mm (Figure 9). The peak of deformation occurs at the back of the bus body, where the battery blocks are located.

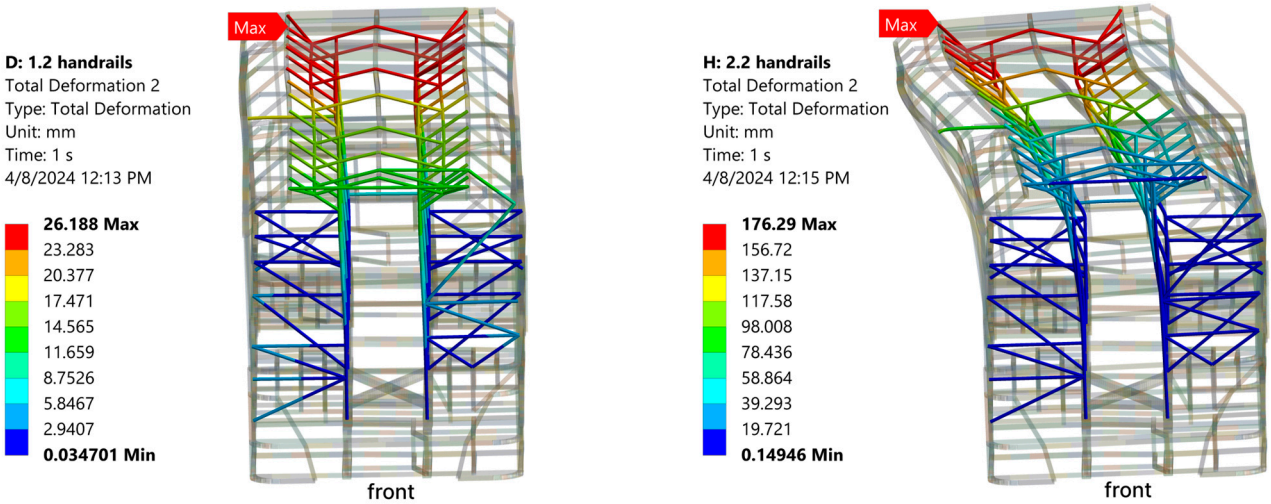

Figure 9. Deformation map of the handrail system in modes: (**a**) #1.2H (air conditioning and gas cylinders load with k_d = 5 and handrails); (**b**) #2.2H (air conditioning and batteries load with k_d = 5 and handrails).

For the purity of the experiment, modes #2.2H and 2.2 (with and without a handrail system) with the same mass of batteries (1875 kg) have been compared. The maximum stress σ_{max} is 380.07 MPa in mode #2.2H (Figure 10a) and 477.95 MPa in #2.2 (Figure 10), which is dangerously close to the ultimate strength of S235 steel. Thanks to the handrail

system integration, the maximum deformations were reduced by 50.3% (from 358.55 to 177.92 mm—Figure 10), which clearly solves the issue of preserving the remaining space of the cabin at the level of the passengers' heads (trapezium according to UNECE R66). The indicator SF_{ave} has grown from 4.84 (mode #2.2) to 7.12 (#2.2H) and the average displacements Δ_{ave} decreased from 64.73 to 37.46 mm, respectively.

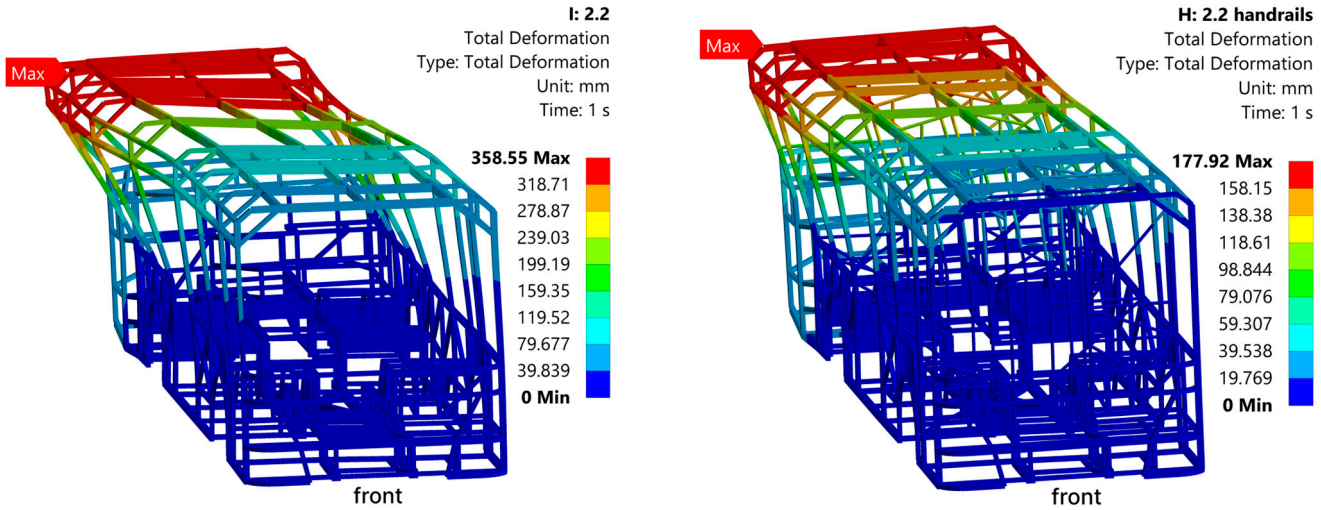

Figure 10. Deformation map in modes: (**a**) #2.2 (air conditioning and batteries load with k_d = 5); (**b**) #2.2H (air conditioning and batteries load with k_d = 5 and handrails).

The modes described above are subject to the requirements of R100/110 and can actually occur only once during the entire period of operation of the bus if the body receives irreversible plastic deformations. Much more widespread in daily operations are vertical accelerations created by road irregularities, which in critical situations can lead to the appearance of k_d = 2.5. The results have been analyzed based on the most loaded mode #3.2 with the battery unit on the roof: σ_{max} is 200.55 MPa in mode #3.2 (Figure 11a) and only 83.09 MPa in #3.2H (Figure 11b). In this case, it is important not only to reduce σ_{max} by 58.57% but also to significantly improve the indicator SF_{min} from 1.25 to 3.01 and Δ_{max} from 9.48 to 4.29 mm.

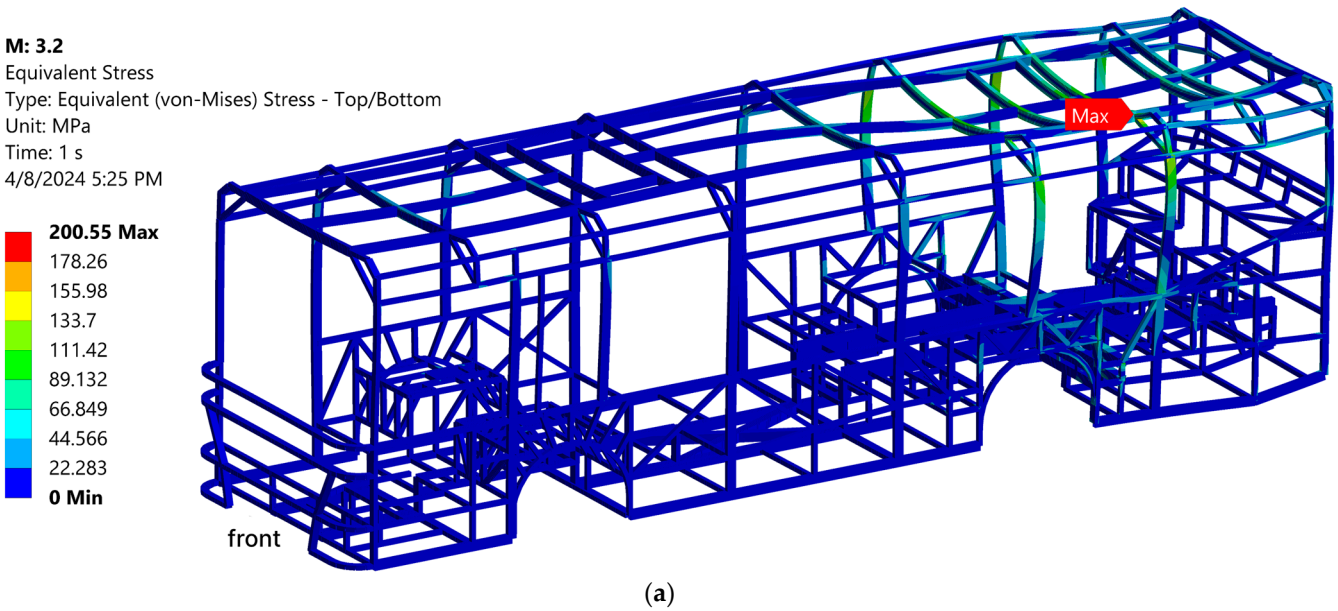

Figure 11. *Cont.*

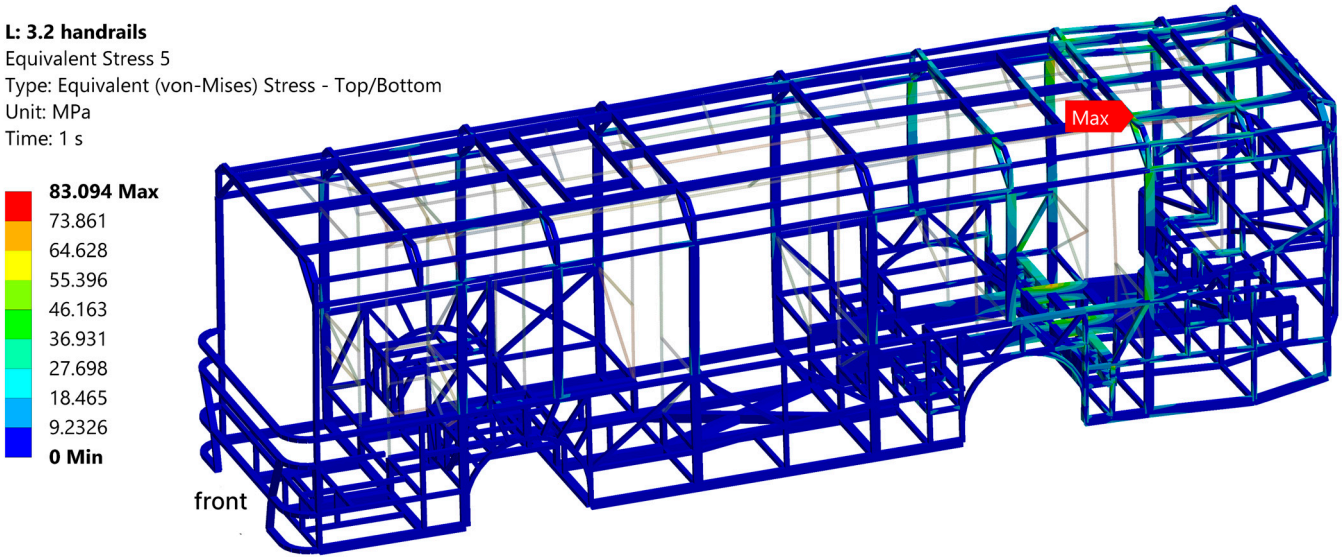

(**b**)

Figure 11. Von Mises stress map in modes: (**a**) #3.2 (air conditioning and batteries load with k_d = 2.5); (**b**) #3.2H (air conditioning and batteries load with k_d = 2.5 and handrails).

The uniform strength SU (mean square deviation of von Mises stresses—σ_{max}, σ_{min}, σ_{ave}) improved almost 2.5 times when switching from mode #3.2 to 3.2H (with the integration of handrails): from 91.21 to 37.89 MPa, respectively.

4. Discussion

The introduction of a welded system of handrails into the body frame not only reduced the maximum and average deformations Δ_{max} and Δ_{ave} but also increased its rigidity and directional stability, which affects the active safety of the bus. Preservation of the geometrical straightness is one of the key factors in the controllability and stability on the road, minimizing bus deviations from the given trajectory of motion. The tendency to curvature of the body along its longitudinal axis is clearly visible on the deformation map in the most complex mode #2.2H (Figure 9b)—the body frame gained a curvilinear shape, destroying the parallelism of the wheel axes and their tracks. The integration of the handrail system enabled the reduction of Δ_{max} from 358.55 mm (mode #2.2) to 177.92 mm (#2.2H), which already affects the issue of passive safety (the penetration of the window racks into the interior volume).

In other test modes, the situation with deformations is significantly easier than in the abovementioned mode #2.2. So, for example, when switching from mode #1.2 to 1.2H, Δmax decreased from 40.71 to 26.95 mm, and when switching from mode #2.1 to 2.1H, 127.88 to 84.66 mm. In the "transverse" modes (#1.2 and 2.2) with the acceleration of 5g, there is a tendency for deformations to increase as they approach the rear wall of the bus body (Figure 10). The longer the rear overhang and the higher the mass concentrated on it (700 kg of gas cylinders in the mode #1.2 or 1875 kg of batteries in the mode #2.2), the greater is the bending moment relative to the rear axle of the bus. Thus, it is recommended to plan the COG of the battery block in the base of the bus during its design.

The reduction in Δ_{max} from 9.48 to 4.29 mm when switching from mode #3.2 to 3.2H is important from the point of view of ensuring the normal daily operation of the bus with its units and aggregates. Thus, caused by road irregularities, cyclical relative displacements of the engine and transmission mounting points of more than 5–10 mm can cause the appearance of dangerous reactions, affecting their durability and reliability.

By comparing the indicators of deformations and stresses in modes #2.1 and 2.2, it can be confirmed that the bus body has a different longitudinal and transverse stiffness. According to the theory, the axial moment of resistance depends on the cross-sectional area, which is significantly different in both directions. Actually, the stress in the upper part of the frame at the acceleration of 5*g* (mode #2.2) is 31.33% higher than in the "longitudinal" mode #2.1 (477.95 vs. 328.23 MPa). The integration of the handrail system in modes #2.2H and 2.1H enabled the reduction in σ_{max} to 380.07 and 301.46 MPa, which is 20.5% and 8.2%, respectively.

The recorded highest stress of 477.95 MPa (mode #2.2) is dangerous in the context of the material's ultimate strength (steel S235 with a limit of ca. 410 MPa). Its popularity is not only due to its financial component but also to its relatively high viscosity, which is especially valuable in the conditions of crash tests: the body frame plastically deforms but does not break up. It should be noted that the mode #2.2H with 380.07 MPa is the next in terms of σ_{max}. Thus, the introduction of the handrail system into the body frame structure protected it from destruction, transferring the maximum stresses to the vicinity of the yield point. Another important positive result is the reduction in σ_{max} from 200.55 MPa (mode #3.2) to 83.09 MPa (#3.2H).

The parameter strength uniformity (SU) proposed in this paper based on the mean square deviation of von Mises stresses (σ_{max}, σ_{min}, σ_{ave}) improved almost 2.5 times when comparing modes #3.2 to 3.2H: from 91.21 to 37.89 MPa, respectively. In general, the topic of future research of SU is of interest to the authors—sectional analysis of the body frame for uniform strength with an integral approach to calculating the total index ΣSU for the entire bus body frame.

From an engineering perspective, the results obtained show that integrating welded handrail elements into the bus body frame can improve the overall rigidity of the structure and redistribute the load within the structure. This approach allows existing interior elements to be integrated into the load-bearing system of the bus body, which can help optimize the design of buses equipped with heavy roof-mounted systems such as batteries or gas cylinders. Since handrails are already mandatory interior elements required by passenger safety regulations, their integration into the welded body frame primarily changes their structural role rather than introducing additional structural components or significant manufacturing complexity. Such integration is also consistent with conventional bus manufacturing practices based on welded steel frame structures and does not significantly increase structural mass or complicate maintenance procedures.

5. Conclusions

1. In order to comply with the numerous safety requirements of the UNECE regulations, the cabin of a modern city bus must be equipped with handrails, which currently perform only one role: ensuring the comfort and safety of passengers. The handrails make up a certain part of the body material capacity, so it has been proposed to provide them with an additional load-bearing function as part of the frame structure, which connects the roof with the floor and binds the sides into a single load-bearing structure. This also increases the structural capacity of the roof frame and facilitates the installation of roof-mounted energy systems used in bus electrification.
2. The results of the integration of the welded handrail system show a possibility of a significant reduction in deformations in each of the modes. Thus, when switching from mode #1.2 to 1.2H, Δ_{max} decreased from 40.71 to 26.95 mm; and from mode #2.1 to 2.1H, from 127.88 to 84.66 mm. The most noticeable are the results for the "transverse" mode with the acceleration of 5*g*: from 358.55 mm (mode #2.2) to 177.92 mm (mode

2.2H), which already affects the issue of passive safety: the penetration depth of the window racks into the cabin volume.

3. The most relevant from the point of view of daily operation are modes #3.1 and 3.2, which involve vertical loads under the action of g with the consideration of k_d to simulate road irregularities. Reduction in Δ_{max} from 9.48 to 4.29 mm when switching from #3.2 to 3.2H ensures normal joint operation of units and aggregates.
4. The situation with σ_{max} is similar to that of the deformations: the higher the loads on the bus body (for example, mode #2.2), the more efficiently the handrail system works (mode #2.2H). The values of σ_{max} decreased from 477.95 to 380.07 MPa, which brings the model out of the critical stress zone above the yield strength (around 250 MPa for steel S235).
5. The proposed index SU of uniform body frame strength based on the mean square deviation of stresses (σ_{max}, σ_{min}, σ_{ave}) confirmed the rationality of the handrail system as part of the load-bearing structure of the body. It improved almost 2.5 times when comparing modes #3.2 and #3.2H: it reduced from 91.21 to 37.89 MPa, respectively.
6. The integration of the welded handrail system solves at least two key engineering tasks: improving structural strength uniformity (SU) and reducing material intensity. All numerical indicators considered in the analysis (deformations, deviations from straightness, SU, and stresses) improved by a factor of two or more. Ideally, the handrail system should approach a biomimetic load-path architecture similar to lattice structures obtained through topological optimization. In such structures, a continuous internal framework forms efficient load paths between the main load-bearing elements of the bus body. In the proposed configuration, the roof, floor, and sidewalls are connected through the handrail system enabling effective load redistribution within the body frame. These results confirm that integrating the welded handrail system as a load-bearing element is a feasible and effective structural solution for improving the stiffness and structural safety of bus body frames.

Author Contributions: Conceptualization: K.H. and M.C.; methodology: K.H. and E.K.; software: K.H.; validation: M.C.; formal analysis: K.H., O.H. and O.D.; investigation: O.D. and I.K.; data curation: A.S. and Y.S.; writing—original draft preparation: K.H. and E.K.; writing—review and editing: M.C. and Y.R.; visualization: R.H. and S.B.; supervision: O.H. and V.R. All authors have read and agreed to the published version of the manuscript.

Funding: This research received no external funding.

Institutional Review Board Statement: Not applicable.

Informed Consent Statement: Not applicable.

Data Availability Statement: The original contributions presented in this study are included in the article. Further inquiries can be directed to the corresponding author.

Conflicts of Interest: The authors declare no conflicts of interest.

References

1. Regulation (EU) 2019/1242, European Commission, Art. 1 (2019). Available online: https://eur-lex.europa.eu/eli/reg/2019/1242/oj/eng (accessed on 15 June 2025).
2. Holenko, K.; Dykha, A.; Voichyshyn, Y.; Horbay, O.; Dykha, M.; Dytyniuk, V. Determining the characteristics of contact interaction between the two-row windshield wiper and a curvilinear glass surface. *East.-Eur. J. Enterp. Technol.* **2024**, *1*, 48–59. [CrossRef]
3. Holenko, K.; Dykha, A.; Posonskiy, S. The influence of the hall effect on the performance of electronic accelerator pedals. In Proceedings of the 2023 IEEE 5th International Conference on Modern Electrical and Energy System (MEES), Kremenchuk, Ukraine, 27–30 September 2023; pp. 1–6. [CrossRef]

4. Holenko, K.; Koda, E.; Kernytskyy, I.; Babak, O.; Horbay, O.; Popovych, V.; Chalecki, M.; Leśniewska, A.; Berezovetskyi, S.; Humeniuk, R. Evaluation of accelerator pedal strength under critical loads using the finite element method. *Appl. Sci.* **2023**, *13*, 6684. [CrossRef]
5. Wang, C.; Yu, H.; Tian, W.; Zhao, C.; Jiang, L.; Bai, Q. Research on the integral forming process of thin walled and thick mouth seamless gas cylinders. *Sci. Rep.* **2023**, *13*, 17021. [CrossRef]
6. Li, Y.; Fang, W.; Lu, C.; Gao, Z.; Ma, X.; Jin, W.; Ye, Y.; Wang, F. Microstructure and mechanical properties of 34CrMo4 steel for gas cylinders formed by hot drawing and flow forming. *Materials* **2019**, *12*, 1351. [CrossRef]
7. Fang, Z.; Wu, G.; Song, C.; Yuan, J.; Wang, Z. Study on the mechanical response of gas cylinders under shock load. In Proceedings of the ASME 2023 Pressure Vessels & Piping Conference, Atlanta, GA, USA, 16–21 July 2023. [CrossRef]
8. Wu, X.; Yang, B.; Zhou, S. Strength and failure analysis of fiber-wound composite gas cylinder via numerical simulation. *Materials* **2024**, *17*, 717. [CrossRef]
9. Park, C.-S.; Jeon, S.-W.; Moon, J.-E.; Lee, K.-J. An explosion of a CNG fuel vessel in an urban bus. *J. Forensic Sci.* **2010**, *55*, 538–541. [CrossRef]
10. Ribeiro, P.J.G.; Dias, G.; Mendes, J.F.G. Public transport decarbonization: An exploratory approach to bus electrification. *World Electr. Veh. J.* **2024**, *15*, 81. [CrossRef]
11. Jie, S.; Jung, T.; Baek, S.; Lee, B. Review: Dynamic force effects on batteries. *J. Acoust. Soc. Korea* **2022**, *41*, 669–679. [CrossRef]
12. Tran, H.N.; Gunawan, F.E.; Pham, N.D. Influence of a nonlinear asymmetric shock absorber on vibration of a bus subjected to harmonic excitation. *J. Vibroeng.* **2023**, *26*, 128–138. [CrossRef]
13. Seong, H.; Sang-Youn, P.; Byoung-Ho, C. Characterization of behavior of lithium ion battery under vibration and shock conditions. *Meet.* Abstr. **2023**, *MA2023-02*, 484. [CrossRef]
14. Haris, A.; Lee, H.P. Vibration, shock and impact analyses of a structural honeycomb battery pack. *Int. J. Crashworthiness* **2023**, *28*, 552–559. [CrossRef]
15. Bharodiya, V.; Sisodia, D.; Singh, P. *Structural Design and Simulation of Battery Enclosure for an Electric Vehicle Against Mechanical Abuse Test*; SAE Technical Paper 2023-28-1345; SAE International: Warrendale, PA, USA, 2023. [CrossRef]
16. Chacko, P.J.; Krishna, S.M.; Nuvvula, R.S.S.; Stonier, A.A.; Kumar, P.P.; Ogale, J.; Khan, B. Estimation of state of charge considering impact of vibrations on traction battery pack. *Electr. Eng.* **2024**, *106*, 1327–1338. [CrossRef]
17. Li, J.; Hou, C.; Xie, M. Analysis of the impact of threshold beam on battery protection based on side impact characteristics. In *Proceedings of China SAE Congress 2023: Selected Papers*; SAE-China 2023. Lecture Notes in Electrical Engineering, Volume 1151; Springer: Singapore, 2024. [CrossRef]
18. Szilassy, P.Á.; Földes, D. Impact of ambient temperature, passenger load, and delay on the consumption of battery electric buses. *Period. Polytech. Transp. Eng.* **2024**, *52*, 113–119. [CrossRef]
19. Gairola, P.; Nezamuddin, N. Design of battery electric bus system considering waiting time limitations. *Transp. Res. Rec.* **2023**, *2677*, 1415–1430. [CrossRef]
20. Yao, C.; Yang, M. Analysis of strength stiffness and modes for bus body frame. *J. Phys. Conf. Ser.* **2021**, *1748*, 062073. [CrossRef]
21. Yang, R.; Zhang, W.; Li, S.; Xu, M.; Huang, W.; Qin, Z. Finite element analysis and optimization of hydrogen fuel cell city bus body frame structure. *Appl. Sci.* **2023**, *13*, 10964. [CrossRef]
22. Wang, P.; Bai, Y.; Fu, C.; Lin, C. Lightweight design of an electric bus body structure with analytical target cascading. *Front. Mech. Eng.* **2023**, *18*, 2. [CrossRef]
23. Pravilonis, T.; Sokolovskij, E.; Kilikevičius, A.; Matijošius, J.; Kilikevičienė, K. The usage of alternative materials to optimize bus frame structure. *Symmetry* **2020**, *12*, 1010. [CrossRef]
24. Fu, C.L.; Bai, Y.C.; Lin, C.; Wang, W.W. Design optimization of a newly developed aluminum-steel multi-material electric bus body structure. *Struct. Multidiscip. Optim.* **2019**, *60*, 2177–2187. [CrossRef]
25. Wang, D.; Xie, C.; Liu, Y.; Xu, W.; Chen, Q. Multi-objective collaborative optimization for the lightweight design of an electric bus body frame. *Automot. Innov.* **2020**, *3*, 250–259. [CrossRef]
26. Zeng, M.; Tan, B.; Ding, F.; Zhang, B.; Zhou, H.; Chen, Y. An experimental investigation of resonance sources and vibration transmission for a pure electric bus. *Proc. Inst. Mech. Eng. D J. Automob. Eng.* **2020**, *234*, 950–962. [CrossRef]
27. Zhang, D.Q.; Zhang, T.X.; Zhao, W.T.; Zhang, W.P. Strength reliability analyses for bus body frames based on Monte Carlo method. In *Advanced Materials Research*; Trans Tech Publications, Ltd.: Baech, Switzerland, 2011; Volume 179–180, pp. 563–568. [CrossRef]
28. Teng, T.L.; Liang, C.C.; Chu, H.M. Development and analysis of bus with composite-material-reinforced frames. *Int. J. Automot. Technol.* **2022**, *23*, 1229–1237. [CrossRef]
29. Barberi, S.; Arena, F.; Termine, F.; Canale, A.; Olayode, I.O.; Neduzha, L.; Zuccalà, Y. Correlations between transportation and the COVID-19 pandemic. In *AIP Conference Proceedings, Proceedings of the International Conference of Computational Methods in Sciences and Engineering (ICCMSE 2021), Heraklion, Greece, 4–7 September 2021*; AIP Publishing: Melville, NY, USA, 2022; Volume 2611. [CrossRef]

30. Voichyshyn, Y.; Popovych, V.; Horbay, O.; Holenko, K.; Dykha, A. Improving Heating of a Bus Interior Using a Combined Heating System. In *Advanced Manufacturing Processes VII. Interpartner 2025*; Tonkonogyi, V., Ivanov, V., Luściński, S., Trojanowska, J., Oborskyi, G., Eds.; Lecture Notes in Mechanical Engineering; Springer: Cham, Switzerland, 2026. [CrossRef]
31. Zelenko, Y.; Zelenko, D.; Neduzha, L. Contemporary principles for solving the problem in noise reduction from railway rolling stock. In *Proceedings of the IOP Conference Series: Materials Science and Engineering, Dnipro, Ukraine, 27–29 May 2020*; IOP Publishing: Bristol, UK, 2020; Volume 985, p. 012015. [CrossRef]
32. Bondarenko, I.; Campisi, T.; Tesoriere, G.; Neduzha, L. Using Detailing Concept to Assess Railway Functional Safety. *Sustainability* **2023**, *15*, 18. [CrossRef]
33. Nguyen, T.C. Research to evaluate the quality of passenger bus body frame, assuring the passive safety in the design process. *Appl. Mech. Mater.* **2019**, *889*, 440–447. [CrossRef]
34. Ruban, D.; Kraynyk, L.; Ruban, H.; Hrubel, M.; Duzhyi, R.; Babaryha, A. Development of technological principles of technical control of bus bodies during operation based on passive safety conditions. *East.-Eur. J. Enterp. Technol.* **2022**, *6*, 91–100. [CrossRef]
35. Holenko, K.; Dykha, O.; Koda, E.; Kernytskyy, I.; Horbay, O.; Royko, Y.; Humeniuk, R.; Sholudko, Y.; Rys, V.; Berezovetskyi, S.; et al. Peculiarities of Assessing Body Strength When Converting a Bus from Diesel to Electric Traction Following the UNECE R100 Regulation. *Appl. Sci.* **2025**, *15*, 8115. [CrossRef]

Disclaimer/Publisher's Note: The statements, opinions and data contained in all publications are solely those of the individual author(s) and contributor(s) and not of MDPI and/or the editor(s). MDPI and/or the editor(s) disclaim responsibility for any injury to people or property resulting from any ideas, methods, instructions or products referred to in the content.